Inorganic Chemistry Communications 127 (2021) 108509

Contents lists available at ScienceDirect

Inorganic Chemistry Communications

journal homepage: www.elsevier.com/locate/inoche

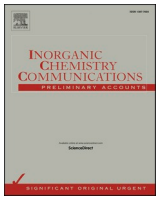

Short communication

Transition-metal complexes of N,N′-di (4-bromophenyl)-4-hydroxycoumarin-3-carboximidamide: synthesis, characterization, biological activities, ADMET and drug-likeness analysis

Drifa Belkhir-Talbi [a,b], Naima Ghemmit-Doulache [b], Souhila Terrachet-Bouaziz [b,c], Malika Makhloufi-Chebli [a,*], Amal Rabahi [d], Lhassane Ismaili [e], Artur M.S. Silva [f]

[a] LPCM Laboratory, Department of Chemistry, Faculty of Sciences, University Mouloud Mammeri, 15000 TiziOuzou, Algeria
[b] Department of Chemistry, Faculty of Sciences, University M'hamed Bouguerra, Boumerdes, Algeria
[c] Laboratory of Applied Organic Chemistry, Faculty of Chemistry, University of Sciences and Technology Houari Boumediene, BP32, El-Alia 16111 Bab-Ezzouar, Alger, Algeria
[d] Laboratoire de Physico-Chimie Théorique et de Chimie Informatique, Faculté de Chimie, USTHB, BP 32, El Alia 16111 Bab-Ezzouar, Alger, Algeria
[e] Laboratoire de Chimie Organique et Thérapeutique, Neurosciences intégratives et cliniques, EA 481, Univ. Bourgogne Franche-Comté, UFR Santé, 19, rue Ambroise Paré, F-25000 Besançon, France
[f] QOPNA, Department of Chemistry, University of Aveiro, 3810-193 Aveiro, Portugal

ARTICLE INFO

Keywords:
Coumarin-carboximidamide
Metal complexes
Antioxidant capacity
Antibacterial activity
Theoretical studies
ADMET drug-likeness

ABSTRACT

Coordination compounds of N,N'-di(4-bromophenyl)-4-hydroxycoumarin-3-carboximidamide (L1) were synthesized via the reaction of Cu (II), Co (II) and Zn (II) salts in molar ratio 1 : 1 in the presence of ammoniac as basic media. The Ligands and the complexes formed were characterized using FT-IR, UV–visible and fluorescence spectrophotometric analyses, mass spectrometry, elemental analyses and NMR spectroscopy. It was concluded that N,N'-di(4-bromophenyl)-4-hydroxycoumarin-3-carboximidamide (L1) coordinated as a mono ligand for all the complexes; it also coordinated via the –OH and –NH groups. The electrochemical behaviour of these compounds was determined by cyclic voltammetry. The synthesized compounds were screened for their antimicrobial and antioxidant activities. All the complexes except that of copper show good activities against the S. *aureus* and those of cobalt and zinc have very interesting diameters of inhibition but lower antioxidant activity than the ligand L1. Parameters drug-likeness and ADMET (Absorption, Distribution, Metabolism, and Excretion) properties have been calculated.

1. Introduction

Metal complexes have been used for a considerable time as pharmaceutical agents, especially in the chemotherapy against cancer [1,2]. More recently, large interest has grown in the use of transition metal complexes [3–6].

On the other hand, Coumarins are an important class of heterocyclic natural products displaying significant biological and pharmacological activities, presenting among others, antibacterial, or antibiotic power (Novobiocin, Clorobiocin). A number of their synthetic analogues have been also reported to be good antifungal and antibacterial agents [7–9]. Preliminary structure–activity relationship studies have shown that the presence of hydroxyl or carboxylic acid derivatives in the coumarin nucleus is necessary to account for the antimicrobial activity [9]. These important potential applications have led to the development of synthetic procedures, either by conventional approaches or by transition metal-catalysis [10–21]. The complexation of coumarins with transition metal ions has been extensively studied [22–29], as they are known to have good complexing ability [30]. The formation of metal complexes with coumarin plays an important role in their reported biological activity. Recently, it has been reported that 4-methyl-7-hydroxycoumarin complexes with several metals show anticoagulants and spasmolytic properties [31,32]. Ferroquine, a metal complex, can produce reactive oxygen species (ROS), which kill the parasites resistant to chloroquine [33]. Considerable effort has now been given to the functionalization of coumarin so that metal-coumarin complexes could be synthesized towards the development of artificial photosynthetic systems, chemical sensors, and molecular level devices [34]. As a result of resistance to

* Corresponding author.
E-mail address: makhloufi_malika@yahoo.fr (M. Makhloufi-Chebli).

https://doi.org/10.1016/j.inoche.2021.108509
Received 23 December 2020; Received in revised form 24 January 2021; Accepted 6 February 2021
Available online 5 March 2021

current drugs and emerging new diseases there is constant need of obtaining antimicrobial and anticancer agents with minimal side effects. The reported widespread applications of the coumarin moiety and their coordination compounds, therefore, informed our interest in the syntheses of novel ligand complexes containing coumarin with the aim of obtaining more potent antimicrobial and cytotoxic agents with possible minimal side effects. Hence, following our studies on the synthesis of coumarins and their transition metal complexes [35], in this work we report the synthesis of a new series of Cu (II), Co (II) and Zn (II) metal complexes derived from compound *N,N'*-di(4-bromophenyl)-4-hydroxycoumarin-3-carboximidamide (**L1**) as well as their antimicrobial and antioxidant activities.

2. Experimental

2.1. Materials and instrumentation

All the chemical reagents and solvents (Fluka products) used were of analytical grade and without further purification. Melting points were determined on a Stuart scientific SPM3 apparatus fitted with a microscope and are uncorrected. The infrared spectra were recorded in the region 4000–400 cm^{-1} on a BRUKER TENSOR 27 IR spectrophotometer. UV–visible spectra were measured on a JENWAY 6800 UV–visible spectrophotometer; measurements were made from 200 to 800 nm. Fluorescence was measured on a JASCO - FP − 8200 spectrofluorometer. The fluorescence quantum yields were determined using fluorescein disodium salt (Φ = 0.90) as standard and calculated using the classical formula:

$$\Phi_X = (\Phi_S.A_S.F_X.n_X^2)/(A_X.F_S.n \quad S2)$$

where "A" is absorbance at the excitation wavelength, "F" the area under the fluorescence curve and "n" is the refractive index of the solvents used. Subscripts "s" and "x" refer to the standard and to the sample of unknown quantum yield, respectively. Proton and Carbon NMR spectra were recorded on a Bruker AC 300 spectrometer (Bruker Biospin). The chemical shifts are expressed in parts per million (ppm) using TMS as internal reference. Mass spectra are obtained with ESI (+) and GC–MS. The elemental microanalysis (C, H, N) was carried out on Truspec 630–200 − 200 Elementary Analysis-Equipment, Service of Microanalysis, Department of Chemistry-University of Aveiro, Portugal. The conductimetric analysis was performed using a Consort C3030 conductivity meter. The compounds were synthesized using method reported by Makhloufi and all [36] with some modifications. Cyclic voltammetry study was carried out in an organic medium DMSO at 25 °C, in the presence of the electrolyte support sodium perchlorate $(NaOClO_4)\cdot 10^{-1}$ M on a Pt disk electrode as a working electrode, the reference electrode was with calomel saturated (ECS) and electrode counters it's a platinum wire (Pt). A scan rate of 100 mVs^{-1} was fixed for all the voltammograms. All solutions were deoxygenated by passing a stream of pre-purified N_2 into the solution for at least 15 min prior to recording the voltammograms.

2.2. Synthesis of ligands and complexes

2.2.1. Synthesis of 4-bromophenyl isothiocyanate

The compound 4-bromophenyl isothiocyanate **2** was synthesized as reported in the literature [37] (scheme 1): To a 250 mL round-bottomed flask, fitted to a magnetic stirrer and a dropping funnel leaving the third neck open and surrounded by an ice-salt cooling bath (10 – 15 °C), the amount of 25.80 g of 4-bromoaniline (0.15 mol) was introduced. To this flsk, 12.37 mL (0.20 mol) of carbon disulfide and 20.00 mL of ethanol were added. The stirrer was started, and 22.50 mL (0.56 mol) of NH_4OH (d = 0.88) was added drop-wise into the mixture from a separatory funnel in about twenty minutes. The temperature of the mixture should be between 10 and 15 °C. The stirring was continued for thirty minutes after all the NH_4OH has been added, and then the reaction mixture was allowed to stand for another thirty minutes at ambient temperature. The milky suspension becomes clear and a heavy precipitate of ammonium 4-bromophenyldithiocarbamate crystallizes. The salt was allowed to stand overnight, then filtered and washed with diethyl ether.

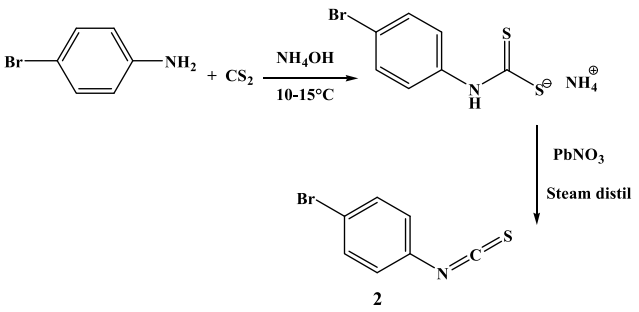

Scheme 1. Synthesis of p-bromophenyl isothiocyanate.

The salt was dissolved in 800 mL of distilled water and transferred to a 2-liter round bottom flask. Aqueous solution of 43.50 g (0.13 mol) of $Pb(NO_3)_2$ dissolved in 87.50 mL of distilled water was added with constant stirring. Lead (II) sulfide separates as a heavy brown precipitate, which soon turned black. The mixture was then distilled with steam (steam distillation), the 4-bromophenyl isothiocyanate **2** was recovered in a flask containing 2.50 mL of 0.5 M sulfuric acid. The latter was separated as white–grey solid and washed with cold water to eliminate traces of sulfuric acid. The yield of 4-bromophenyl isothiocyanate was 39% (12.42 g) and melting point 61 °C (reported 50%, 61 °C [37]).

2.2.2. Syntheses of ligands N,N'-di(4-bromophenyl)-4-hydroxycoumarin-3-caroximidamide (L1) and of N-4-bromophenyl-4-hydroxycoumarin-3-carbothioamides (L2)

A mixture of 0.81 g (5 mmol) of 4-hydroxycoumarin **1** and 0.8 mL (5 mmol) of triethylamine dissolved in 10.0 mL of DMSO was stirred during 15 mn and then 15.00 mmol of 4-bromophenyl isothiocyanate was added. The reaction mixture was stirred at room temperature for 15 h, 50.0 mL of cold water was added followed by treatment with a mixture of diethyl ether-light petroleum (1:1). The solid precipitate formed was recrystallized from isopropyl alcohol giving *N,N'-di*(4-bromophenyl)-4-hydroxycoumarin-3-carboximidamide **L1** (1.15 g, 45%).

The aqueous layer was acidified with HCl 1 N (pH = 4–5) and the precipitate thus formed was collected by filtration and washed several times with cold water. The solid was recrystallized from isopropyl alcohol giving N-4-bromophenyl-4-hydroxycoumarin-3-carbothioamide **L2** (659.80 mg, 35%).

2.2.2.1. N,N'-di(4-bromophenyl)-4-hydroxycoumarin-3-carboximidamide (L1). White Powder, mp 235–236 °C; ^{1}H NMR ($CDCl_3$): δ 6.74 (d, 2H, *J* = 9.6 Hz, ArH), 7.17 (d, 2H, *J* = 8.7 Hz, ArH), 7.28 (d, 1H, *J* = 9.3 Hz, ArH), 7.31 (d, 2H, *J* = 8.7 Hz, ArH), 7.37 (t, 1H, *J* = 9.3 Hz, ArH), 7.55 (d, 2H, *J* = 9.6 Hz, ArH), 7.69 (t, 1H, *J* = 9.3 Hz, ArH), 8.12 (d, 1H, *J* = 9.3 Hz, ArH), 13.35 (s, 1H, NH), 17.46 (s, 1H, OH); ^{13}C NMR ($CDCl_3$): δ 89.4, 97.4, 116.1, 122.2, 123.8, 124.5, 124.7, 126.9, 131.3, 135.7, 149.2, 151.6, 158.7, 162.7, 166.0, 174.3, 180.2, 189.5; ms (EI): *m/z* 512 (40), 449 (9), 447 (10), 359 (18), 357 (20), 216 (15), 215 (100), 214 (15), 213 (99), 183 (3.9), 181 (4), 158 (2.5), 156 (3), 155 (25), 143 (2), 134 (50), 117 (2), 107 (9), 76 (8). Anal. Calcd. for $C_{22}H_{14}Br_2N_2O_3$ (514.17): C, 51.39; H, 2.74; N, 5.45. Found: C, 51.54; H, 2.850; N, 5.81.

2.2.2.2. N-(4-bromophenyl)-4-hydroxycoumarin-3-carbothioamide (L2). Yellow powder, mp 270–271 °C; ^{1}H NMR ($CDCl_3$): δ 6.75 (d, 2H, *J* = 9.8 Hz, ArH), 7.17 (d, 2H, *J* = 9.8 Hz, ArH), 7.31 (t, 1H, *J* = 9.0 Hz, ArH), 7.37 (d, 1H, *J* = 9.0 Hz, ArH), 7.69 (t, 1H, *J* = 9.0 Hz, ArH), 8.12 (d, 1H, *J* = 9.0 Hz, ArH), 13.34 (s, 1H, NH), 17.45 (s, 1H, OH); ^{13}C NMR ($CDCl_3$): δ 97.3, 116.0, 123.7, 125.3, 126.8, 131.2, 131.7, 134.7, 135.7,

136.0, 151.5, 162.7, 179.4 (C-OH), 188.4 (C = S); ms (ESI+): *m/z* 400 [26, $(M + Na)^+$, ^{81}Br], 398 [29, $(M + Na)^+$, ^{79}Br], 378 [96, $(M + H)^+$, ^{81}Br], 376 [100, $(M + H)^+$, ^{79}Br]. Anal. Calcd. for $C_{16}H_{10}BrNO_3S$ (376.23): C, 51.08; H, 2.68; N, 3.72. Found: C, 51.29; H, 2.84; N, 3.65.

2.2.3. Syntheses of Cu (II), Zn (II) and Co (II) complexes of ligand L1

The complexes of ligand **L1** were prepared from metal chloride salts of copper, cobalt and zinc as follows:

To an ethanolic solution containing 0.50 mmol of $MCl_2{\cdot}xH_2O$ (M = Cu (II), Co (II) and Zn (II)) dissolved in 5.00 mL was added 0.50 mmol (0.257 g) of L1 dissolved in a mixture ethanol- chloroform (10.00 mL/ 20.00 mL). NH_4OH was then added while adjusting the pH to 7–8 and the mixture was refluxed for 6 h until formation of precipitate. The solid precipitate formed was collected by filtration, washed with hot ethanol and hot chloroform and dried.

2.3. Screening for antibacterial activity by the agar diffusion method for L1 and its transition metal complexes

The antimicrobial activities of ligand L1 and its Cu (II), Co (II), and Zn (II) complexes were evaluated for their antibacterial activities against *Escherichia coli* (ATCC 25922), *Pseudomonas aeruginosa* (ATCC 27853) and *Staphylococcus aureus* (ATCC 25923) by the agar diffusion method [38]. A sterile physiological water solution contained bacterial colonies, was prepared at room temperature, with an optical density of 0.08–0.10 corresponding to a concentration of 106 cells/mL. The bacterial solution was inoculated in the Muller-Hinton agar medium by swabbing using Petri dishes at room temperature. The tested compounds were dissolved in dimethylsulfoxide (DMSO) with a concentration of 5.00 mg/mL. Twenty-five microlliters of tested sample were poured onto filter paper discs 6 mm in diameter, which were then delicately placed on the surface of the agar plates. These were later maintained at 37 °C for 24 h. Activities were determined by measuring the diameter of the inhibition zone (mm).

2.4. Antioxidant activity

The antioxidant activity of the synthesized L1 and its complexes was evaluated using the 2,2-diphenyl-1-picrylhydrazyl free radical (DPPH·) scavenging assay [39,40]. DPPH· solution was prepared by dissolving DPPH· in ethanol to give a concentration of 4.00 mg/100 mL. Compounds L1, $[Zn(L1)(NH_3)_2Cl_2]H_2O$, $[Cu(L1)(NH_3)_2Cl_2]H_2O$ and $[Co(L1)(NH_3)_2Cl_2]H_2O$ were dissolved in DMSO to obtain solutions of 1.00×10^{-1} M. The concentration of test compounds was diluted with DMSO to get final concentrations 5.00×10^{-2}, 25.00×10^{-3} and 12.50×10^{-3} mol/L for all the compounds. The standard was further diluted to give concentration solutions of 1.00×10^{-1}, 5.00×10^{-2}, 25.00×10^{-3} 12.50×10^{-3}, 6.25×10^{-3}, 31.25×10^{-4} and 15.63×10^{-4} mol/L. To 40 μL of each concentration of tested compounds was added 2.00 mL of DPPH solution. The mixtures were incubated in the dark at room temperature for 1 h and then the absorbances were measured at 517 nm. Ascorbic acid (AA) was used as standard for the antioxidant activity screening and a blank containing only ethanol with DMSO was used as the control. DPPH scavenging effect was calculated as percentage of DPPH discoloration using the equation:

$$RSA\ (\%) = [(Ac - As)/Ac] \times 100 \quad (1)$$

where **Ac** was the absorbance of the control (absorbance of DPPH ethanol solution without sample), and **As** was the absorbance of the tested compound after 60 min incubation.

All the tests were made in duplicate and at least two different assays were performed for each sample.

2.5. Theoretical study

In order to establish theoretically the coordination sites and make a comparison with the experimental observations, quantum chemical calculations of Mulliken atomic charges have been carried out. For this, the 2D structures of synthesized ligands and metallic complexes were drawn with Marvin Sketch [41]. The geometries optimization and frequencies calculation were calculated using ORCA, an electronic structure program package [42,43] at density functional theory (DFT) using standard Becke's three-parameter hybrid model, Lee–Yang–Parr (B3LYP) functional and 6-31G** [44,45] and LANL2DZ basis sets, for ligand L1 and synthesized metallic complexes, respectively. Since the density functional theory (DFT) was not able to describe long-range London dispersion interactions, we corrected the local density with the original D3 damping function [46]. In order to perform a comparative study of the stability of the synthesized metallic complexes, we calculated the Binding Energy (BE), which is given by:

$$E_{binding} = E_{complex} - (E_{metal} + E_{ligand}) \quad (2)$$

where, $E_{complex}$ is the energy of the optimized complex and $\mathbf{E_{Ligand}}$ is the single point energy of ligand in the optimized one. The highest BE corresponds to the most stable complex. UV–visible, IR spectra and deformation electron density were generated using Gabedit 2.5.0 [47] and Multiwfn [48].

2.6. ADMET and drug-likeness analysis

The ADMET (absorption, distribution, metabolism, excretion, and toxicity) properties of molecules describe their disposition within an organism [49]. Therefore, it was necessary to use the computational tools to predict ADMET properties which used only the molecular structure [50]. Several studies using in silico ADMET properties analysis were reported in the literature [35].

In this context, admetSAR [51] and SwissADME [52] servers were used to predict AMES toxicity (AMEST) [53], Carcinogenicity [54], Human Ether-a-go-go-Related Gene (hERG), P-glycoprotein inhibition (PG Inhibitors) [55], inhibition of four cytochrome P450 isoforms (CYP2C19, CYP2D6, CYP3A4 and CYP450 2C9) [56], Blood-brain barrier (BBB) permeability [57], and human intestinal absorption (HIA) [58], CaCo-2 permeability (PCaco-2) [59]. Some physicochemical properties were also evaluated such as Log P and TPSA.

3. Results and discussion

The condensation of 4-hydroxycoumarin **1** with 4-bromophenylisothiocyanate **2** in the presence of triethylamine as basic catalyst in DMSO as solvent at room temperature for 15 h, led to the formation of two compounds **L1** and **L2** (see scheme 2) [36].

The IR spectrum of L1 showed strong peaks at 1670 and 1609 cm^{-1}, corresponding respectively to the carbonyl C = O and imine C = N groups of the coumarin ring. The –OH and –NH groups displayed absorptions around 3126 and 3066 cm^{-1} respectively [36].

The mass spectra of compounds L1 indicated that the coumarin ring was conserved, confirmed by the observed peaks at *m/z* 134, 143 and 117 corresponding to the fragmentation of the coumarin ring [60,61]. The elemental analysis and the mass spectra of L1 indicated the absence of sulfur in the structure and that two molecules of 4-bromophenyl isothiocyanate **2** reacted with **1**.

The ^1H NMR spectra showed the presence of signals corresponding to the resonances of two exchangeable protons at δ 13.35 and 17.46 ppm, assigned to the –NH and –OH groups respectively. The ^{13}C NMR spectra showed that compound L1 exist as a mixture of two tautomers (Scheme 2 and Fig. 11). In fact L1 displayed two signals for the resonance of carbons 3 (δ 97.4 and 116.1 ppm), C-4 (δ 179.6 ppm assigned to C-OH; δ 188.5 ppm assigned to C = O) and C-9 (δ 166.0 ppm assigned to = C

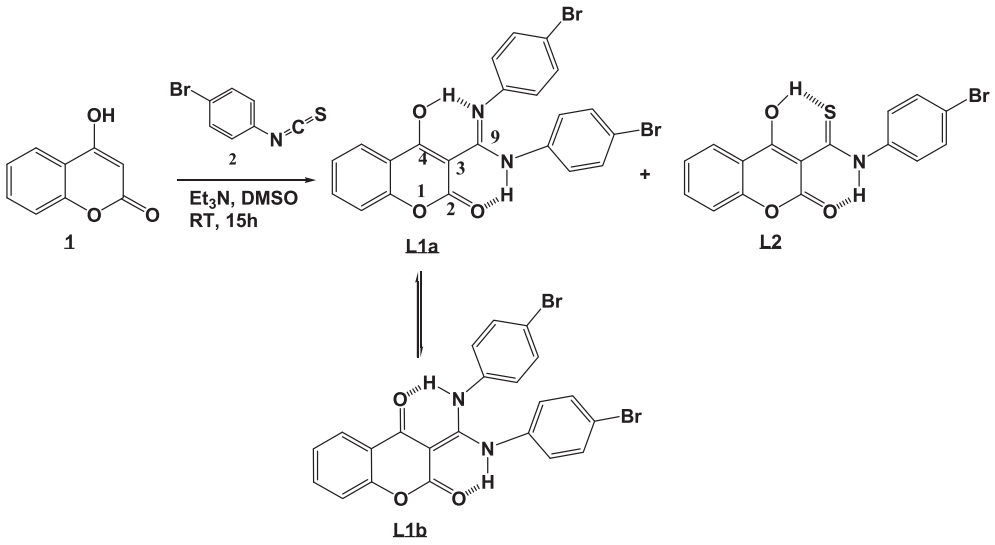

Scheme 2. Synthesis of the ligands L1 and L2.

$(NHAr)_2$; δ 179.6 ppm assigned to -C(NHAr) = NAr and the signals of the aromatic carbon]: C-3 (δ 97.4 and 116.1 ppm) and C-4 (δ 179.6 ppm assigned to C-OH; δ 188.5 ppm assigned to C = O) (see experimental section).

The ^{1}H NMR spectra of L2 showed two singlets at δ 13.34 and 17.45 ppm corresponding to the resonance of –NH and –OH groups, whereas the ^{13}C NMR spectra show a characteristic carbothiamoyl signal at δ 188.40 ppm (C = S) (see experimental section and ref [36]).

3.1. UV–Visible spectroscopic study

3.1.1. Absorption spectrum titrations of L1 and L2 with Cu^{2+}

To optimize the complexation, a study was carried out to determine the molar ratio M/L required for the synthesis of the complexes. Thus, the solutions of the ligands and metal were prepared in DMSO at concentrations of $6x10^{-5}$ M.

The absorption spectrum of the free ligands L1 and L2 was studied. In the case of L1, the weak wavelength at 268 nm was attributed to the n-π* transition of the imine group and the intense long-wavelength band situated around 337 nm was attributed to the π–π* transition of the coumarins' carbonyl group. Addition of $CuCl_2$ to a solution of L1 ($6x10^{-5}$ M) in DMSO induced drastic changes in the absorption spectrum. A strong hypochromic effect on the short-wavelength band at 268 nm (Fig. 1-A, curves a to i) was observed. The band around 337 nm underwent a hypochromic effect, lost its plateau shape and shifted to the red. The same effect was observed for the three investigated cations.

For L2, the intense long-wavelength band situated around 358 nm was attributed to the π–π* transition of the carbonyl group and the weak one at 268 nm which appears as a shape was attributed to the n-π* transition of the carbothionyl group. The addition of $CuCl_2$ to a solution of L2 ($6x10^{-5}$ M) in DMSO induced drastic changes in the absorption spectrum. A strong hypochromic effect on the wavelength band at 358 nm and on the shape at 268 nm (Fig. 1-B, curves a to i) was observed.

Then, the absorbance as a function of cation concentration was analysed (Figs. 2A and 2B). As the shape of the absorption spectrum varied strongly in the presence of cations, the absorbance was recorded at two different wavelengths chosen in order to obtain maximum information. For each salt, the calculation was performed simultaneously on the two bands obtained by absorption spectroscopy there by giving good fits, as displayed in Fig. 2.

The results of Fig. 2 showed that from an equimolar ratio metal/ligand, the absorbance becomes constant. The time factor on metal–ligand coordination (1:1) of L1/Cu^{2+} is also studied. Hypochromic effect on the wavelength band at 337 nm is observed (Fig. 3, see supplementary information).

3.1.2. Effect of the nature of metal

The effect of the nature of metal has also been studied (see supplementary information). The results showed that the absorbance and the wavelength were much affected by the presence of the metal. The various metal ions (Mn^{2+}, Co^{2+}, Ni^{2+} and Zn^{2+}) caused absorption spectra changes of **L1** and **L2**.

The zinc, nickel, manganese and the cobalt ions shift the wavelength towards the red whereas the copper towards the blue (Fig. 4-A and B, see supplementary information). In this regard, **L1** and **L2** exhibit satisfying selectivity for transition metal ions M^{2+}. The absorption characteristics are collected in Table 1 ans Beer-Lambert's law was satisfied in the range of concentration studied ($6x10^{-5}$ M). The molar extinction coefficient was measured at the CT band maximum. For compound **L1** and **L2**, it was found to be equal to 23,953 and 23428 M^{-1} cm^{-1} respectively (Table 1). In contrast, addition of metal cations, induced a hypochromic and hypsochromic (only Cu^{2+})/batochromic (other cations) shift on the CT band (Fig.4, see supplementary information). The molar extinction coefficient decreases upon addition of metal cation M^{2+} indicating in this case, that the CT bands also decreased.

3.2. Effect of pH on the absorption spectra of the ligands L1 and L2

A UV–visible spectrophotometry study of the effect of pH on the displacement of the ligands L1 and L2 wavelengths was carried out in order to optimize the pH value affecting the absorption wavelength of the coumarin nucleus. The pH change was made by the addition of ammoniac to solutions of L1 and L2 ligands dissolved in DMSO at concentrations of 6.00×10^{-5} M. As shown in Fig. 5 (see supplementary information) the pH showed an effect on the absorption spectra of L1 and L2. In fact initially, the pH value recorded for 6.00×10^{-5} M ligands solutions is of the order of 6–7 units and the addition of the ammoniac drops gave rise to a pH variation. A slight Hyperchromic displacement of the absorption wavelength at 337 nm attributed to coumarin was observed for L1. Concerning L2 hypochromic and batochromic displacements at 268 and 358 nm was observed. From pH 8 no variation was observed on the spectrums, involving that the base did not affect the ligands and that there was no interaction between the L1 and L2 ligands and the ammonia as well as no deprotonation of the hydroxyl groups.

The effect of the addition of ammonia on the equimolar mixture L1/$CuCl_2$ was also studied by UV–visible analysis (Fig. 6, see supplementary

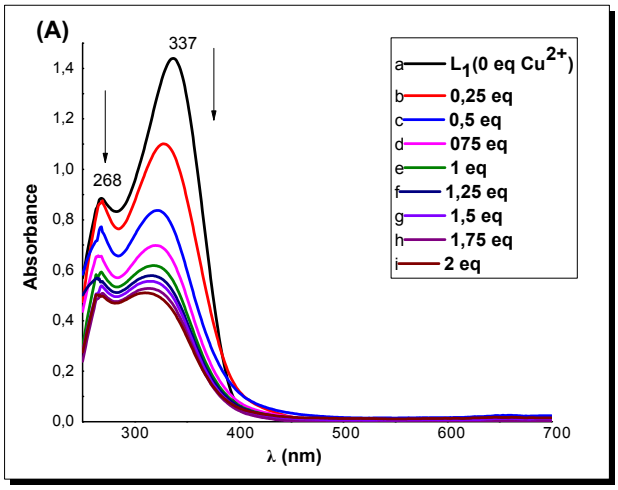

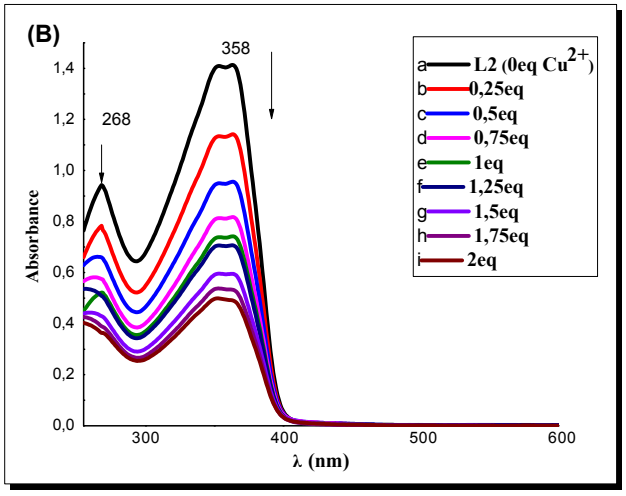

Fig. 1. (A) Absorption spectrum of L1 ($6x10^{-5}$ M) in DMSO in the absence (curve a) and presence of increasing amounts of $CuCl_2$: Curves b to i: effect of $CuCl_2$ addition. From top to bottom at 268 nm and 337 nm: $CuCl_2$ ($6x10^{-5}$ M): 0.00; 0.25; 0.50; 0.75; 1.00; 1.25; 1.50; 1.75 and 2.00 equivalents **(B)** Absorption spectrum of L2 ($6x10^{-5}$ M) in DMSO in the absence (curve a) and presence of $CuCl_2$. Curves b to i: effect of $CuCl_2$ addition. From top to bottom at 268 nm and 358 nm: $CuCl_2$ ($6x10^{-5}$ M): 0.00; 0.25; 0.50; 0.75; 1.00; 1.25; 1.50; 1.75 and 2.00 equivalents.

information). The results showed a variation on the absorption wavelength after addition of ammonia and remain unchangeable after pH 7–8.

3.3. Fluorescence spectra study

3.3.1. Effect of the stoichiometric amount of the metal on the ligands

On the other hand, the fluorescence spectra of L1 and L1 + Cu^{2+} were also recorded in the optimized experimental condition. In the absence of $CuCl_2$, the emission spectra of L1 ($6x10^{-5}$ M, $\lambda_{ex} = 337$ nm) in DMSO showed only one band with maxima situated at around 423 nm Stokes shift equal to 6033 cm^{-1}. In the presence of $CuCl_2$, and with the same excitation wavelength (Fig. 7-A), the results showed that the intensity emission peaks at 423 nm increases with the addition of Cu^{2+} and the fluorescence intensity becomes constant at an equimolar ratio metal/ligand, indicating the formation of L1-Cu^{2+} complex.

In the case of **L2**, the emission spectra ($6x10^{-5}$ M, $\lambda_{ex} = 358$ nm) in DMSO showed one band with maxima situated at around 408 nm wavelength. In the presence of $CuCl_2$, and with the same excitation

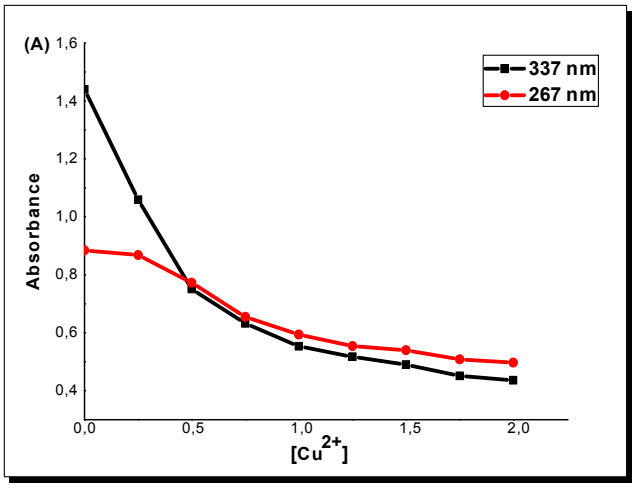

Fig. 2A. Fitted spectrophotometric data for compound L1 in DMSO vs. cation concentration. Variation of absorbance: λ = 267 and 337 nm.

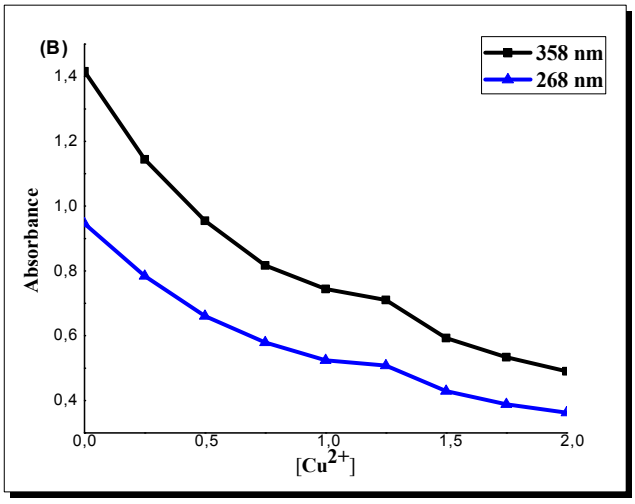

Fig. 2B. Fitted spectrophotometric data for compound L2 in DMSO vs. cation concentration. Variation of absorbance: λ = 268 and 358 nm.

Table 1
Spectroscopic characteristics of **L1** and **L2** in the absence and in the presence of different transition metal ions: Maximum absorption wavelength of the CT Band ($\lambda_{abs\ max}$) and apparent molar extinction coefficient at the absorption maximum (ε).

Ligand	Ion	$\lambda_{abs\ max}$ (nm)	ε (M^{-1} cm^{-1})
L1	/	337	23,953
	Co^{2+}	343	12,913
	Cu^{2+}	321	11,672
	Ni^{2+}	343	11,672
L2	/	358	23,428
	Co^{2+}	354	09,906
	Cu^{2+}	322	08,073
	Ni^{2+}	354	09,822
	Zn^{2+}	354	09,913
	Mn^{2+}	358	10,090

wavelength (Fig. 7-B), the results showed that the intensity emission peaks at 408 nm decreases with the addition of Cu^{2+} and the variation of the fluorescence intensity becomes very weak from an equimolar ratio metal/ligand, indicating the formation of L1-Cu^{2+} complex.

Ligands **L1** and **L2** exhibited quantum yields of 0.031 and 0.078

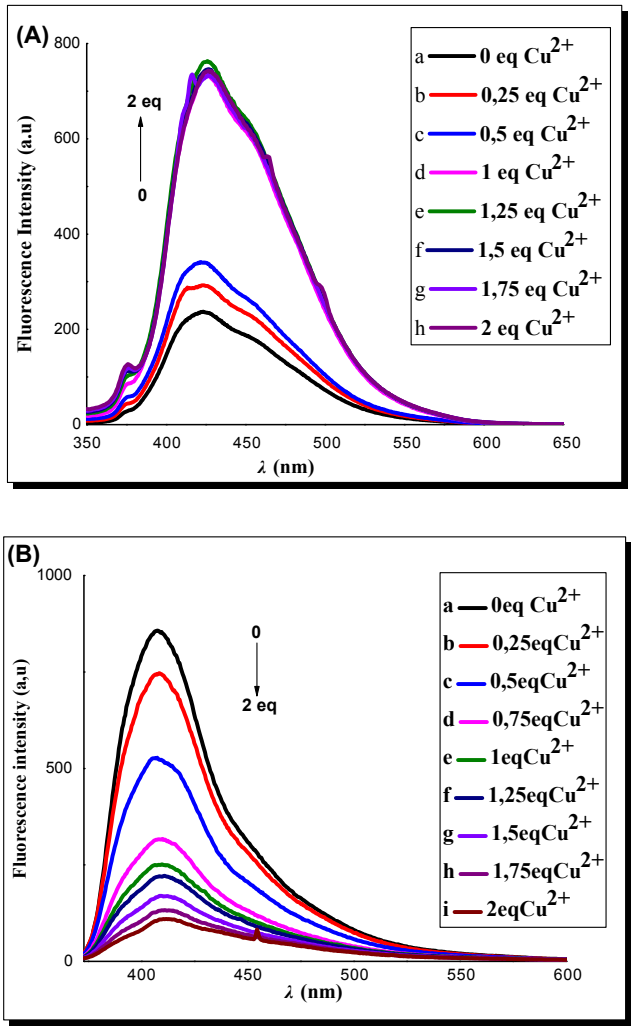

Fig. 7. (A): Fluorescence emission spectra of L1 ($6x10^{-5}$ M, in DMSO) in the absence (curve a) and presence of increasing amounts of $CuCl_2$: Curves b to h: effect of $CuCl_2$ addition. From bottom to top at 423 nm: $CuCl_2$ (6.10^{-5}M): 0.00; 0.25; 0.50; 0.75; 1.00; 1.25; 1.50; 1.75 and 2.00 equivalent. Excitation wavelength 337 nm. (B): Fluorescence emission spectra of L2 ($6x10^{-5}$ M, in DMSO) in the absence (curve a) and presence of increasing amounts of $CuCl_2$: Curves b to i: effect of $CuCl_2$ addition. From top to bottom at 408 nm: $CuCl_2$ ($6x10^{-5}$M): 0.00; 0.25; 0.50; 0.75; 1.00; 1.25; 1.50; 1.75 and 2.00 equivalent. Excitation wavelength 358 nm.

respectively. The presence of Cu^{2+} ion increase the quantum yield of L1 and decrease the one of L2. Fitted spectrofluorimetric data for compounds L1 and L2 in DMSO vs. cation concentration (Fig. 8, A-B, see supplementary information) showed that from an equimolar ratio metal/ligand, the intensity becomes constant.

3.3.2. Effect of the nature of metal

The effect of the nature of metal on the emission spectra has also been studied. The results showed that the presence of the metal affects the intensity more than the emission wavelength, except for the copper where the emission wavelength was displaced and a bathochromic effect was observed (Fig. 9-A and B, see supplementary information).

The effect of the addition of ammonia on the equimolar mixtures L1-MCl_2 and L2-MCl_2 at pH 7–8 was also studied (see Fig. 10-A and B, supplementary information). The results showed a variation on the emission spectrum and the intensity becomes more important.

3.4. Characterization of the complexes

3.4.1. Elemental analyses

The elemental analyses data agreed well with the proposed formula for the metal (II) complexes. The results showed a 1:1 (metal : ligand) stoichiometry and the appearance of a high percentage of nitrogen indicating its presence in the complex. The analytical results are in good agreement with those required mole ratio for the general formula [ML$(NH_3)_2Cl_2$].H_2O. Table 2 summarized the results obtained for the elemental analyses.

3.4.2. NMR study of the complexes

The proton NMR spectra of the free ligand **L1** (Fig. 11, see supplementary information) and the complexes (Fig. 12, see supplementary information) were recorded in $CDCl_3$ and DMSO-d_6 respectively. Comparison of the spectra of the complex with the ligand **L1** revealed that the resonances were considerably broadened and also shifted on complexation. The ^{1}H NMR spectrum of the zinc complex proton (Fig. 12) showed that the peak of the –NH and –OH groups were conserved, which implied the conservation of the latter. The spectroscopic variations suggested that definite interactions took place between ligand and metal cation. The peak of –OH group is more shifted than the –NH group which implied its participation in the complexation. The ^{1}H NMR spectrum of L1 complexes at saturation in DMSO showed very weak shifts on the peaks corresponding to the aromatic protons. Additional techniques were used to provide more information about the structure of the complexes.

3.4.3. Infrared

Infrared spectra are the most suitable technique to determine the coordinating atoms of the ligands by comparing the free ligand spectra with those of the complex. The Table 3 summarized the results obtained by IR analysis (see Supplementary material section).

A careful study of IR spectra of Cu (II), Co (II) and Zn (II) complexes, and a comparison with the ligand L1, showed that the band corresponding to –OH stretch was affected by complexation and shifted to higher frequencies in both complexes. In addition, the stretching vibration band of the –NH of the carboximidamide ring was weakened and shifted to 3052 cm^{-1}, 3100 cm^{-1} and 3050 cm^{-1} for the Cu (II), Co (II) and Zn (II) complexes respectively. The stretching vibration band of the carbonyl bond of the pyronic ring was weakened and shifted to 1652–1659 cm^{-1} for all the complexes and less affected by the nature of the metal. This later band was observed as an intense band, suggesting that the carbonyl-group was not coordinated with the metal. These variations were also found for the imine vibration band C = N of carboximidamide. The results are in favor of metal–ligand interactions through the oxygen atom of pyronyl hydroxyl –OH and –NH of carboximidamide. New broad bands appear at 3500 cm^{-1}, 3550 cm^{-1} and at 3400 cm^{-1} for the copper, cobalt and zinc complexes respectively, probably due to water [62] indicating the presence of the latter in the chelates.

The spectrum of the complexes also exhibited a broad band at 2942 cm^{-1} (CuL1), 2962 cm^{-1} (CoL1) and 2992 cm^{-1} (ZnL1), related to $–NH_3$ bonded [63] suggesting that ammoniac had not deprotonated the –OH group but it participated in the coordination. Apparition of new peaks due to the M–O and M–N bonds of the complexes [64,65] signify the coordination of L1 with Cu (II), Co (II) and Zn (II) cations. The characteristics of the FTIR spectra of all complexes were in agreement with the suggested structural formula.

3.4.4. Electronic spectra

The UV–visible absorption spectra of the three complexes are shown in Fig. 13A-C and Table 4 below summarizes the results obtained for the electronic absorption bands of complexes.

The UV–visible absorption spectrum of the complex [Cu(L1)$(NH_3)_2Cl_2$]H_2O (Fig. 13-A, see supplementary information) showed in

Table 2
Elemental analyses data of the investigated compounds.

Complex	C%		H%		N%		Cl %	
	Calcd.	Found	Calcd.	Found	Calcd.	Found	Calcd.	Found
$[Zn(L1)(NH_3)_2Cl_2]H_2O$	38.50	38.33	3.51	3.44	7.81	7.61	9.88	10.12
$[Co(L1)(NH_3)_2Cl_2]H_2O$	38.85	38.96	3.54	3.72	7.88	7.68	9.97	9.83
$[Cu(L1)(NH_3)_2Cl_2]H_2O$	38.60	38.49	3.52	3.75	7.83	7.95	9.91	10.09

Table 3
Relevant infrared spectra bands for the ligand and complexes (cm^{-1}).

Comp.	v(OH)	$\bar{\nu}(H_2O)$	$\bar{\nu}(NH_3)_{as}$	$\bar{\nu}(C=O)$	$\bar{\nu}(C=N)$	$\bar{\nu}(NH)$	$\bar{\nu}(M-O)$	$\bar{\nu}(M-N)$
L1	3132	–	–	1670	1609	3088	–	–
$[Zn(L1)(NH_3)_2Cl_2]H_2O$	3152	3400	2992	1652	1602	3050	522	495
$[Cu(L1)(NH_3)_2Cl_2]H_2O$	3256	3500	2942	1657	1602	3052	559	442
$[Co(L1)(NH_3)_2Cl_2]H_2O$	3220	3550	2962	1656	1602	3100	494	446

Table 4
Electronic spectral data of the complexes recorded in DMSO.

Samples	λ (nm)	$\nu(cm^{-1})$	Transitions
$[Zn(L1)(NH_3)_2Cl_2]H_2O$	274	36,496	n → π*
	342	29,240	π → π*
	415	24,096	MLTC
$[Cu(L1)(NH_3)_2Cl_2]H_2O$	268	37,313	n → π*
	338	29,586	π → π*
	411	24,331	MLTC
	530	18,868	$^2B_1g \rightarrow {}^2Eg$
	590	16,949	$^2B_1g \rightarrow {}^4A_1g$
$[Co(L1)(NH_3)_2Cl_2]H_2O$	267	37,453	n → π*
	346	28,902	π → π*
	436	22,936	MLTC
	551	18,179	$^4T_1g \rightarrow {}^4T_1g(P)$
	645	15,505	$^4T_1g \rightarrow {}^4T_2g(F)$

the ultraviolet domain two bands located at 37313 cm^{-1} and at 29586 cm^{-1} respectively. The latter were due to the intra ligand transitions n → π* and π → π* respectively. Another band located at 24331 cm^{-1} as a shoulder corresponded to the metal–ligand charge transfer. Two bands appear in the visible at 16949 cm^{-1} and at 18868 cm^{-1} corresponding to transitions $^2B_1g \rightarrow {}^2A_1g$ and $^2B_1g \rightarrow {}^2Eg$. These electronic transitions were characteristic of an octahedral geometry [66].

The electronic absorption spectra of the complex $[Co(L1)(NH_3)_2Cl_2]H_2O$ (Fig. 13-B, see supplementary information) showed two bands located at 37453 cm^{-1} and 28902 cm^{-1} due to the transitions n → π* and π → π* respectively. A shoulder appears at 22936 cm^{-1} corresponded to the metal–ligand charge transfer (CT). Two new bands appear in the visible at 18149 cm^{-1} and at 15504 cm^{-1} were attributed to the $^4T_1g \rightarrow {}^4T_1g(P)$ and $^4T_1g \rightarrow {}^4T_2g(F)$ transitions respectively. These correspond to an octahedral geometry [67].

The spectra of $[Zn(L1)(NH_3)_2Cl_2]H_2O$ (Fig. 13-C, see supplementary information) have been shifted towards the high wavelengths at 36496 cm^{-1} and 29240 cm^{-1}, which showed ligand engagement in complex formation. A new wavelength at 24096 cm^{-1} was attributed to the charge transfer of the metal–ligand. The absorption spectrum exhibited no band in the visible region of the spectrum. No d-d absorption band was observed in the visible region. This is partly due to the fully filled 3d of Zn (II) ion. An octahedral geometry is proposed for this complex [68].

3.5. Complex structures and theoretical studies

All geometries of synthesized ligand L1 (A and B) were optimized with density functional theory (DFT) using Becke's three-parameter hybrid model, Lee–Yang–Parr (B3LYP) [44,45] with 6-311G** using ORCA program [42,43]. Frequency analysis was performed at the same level of theory. Quantum chemical calculations of Mulliken atomic charges have been carried out in order to determine theoretically the coordination sites and make a comparison with the experimental observations.

Fig. 14 represents the optimized geometries of the ligand L1 as well as the charge density values calculated. It has been found that the highest negative values were those of the oxygen hydroxyl group (−324) and the nitrogen of –NH group (−457), suggesting that the latter favor more the coordination with the transition metals.

Time-Dependent Density Functional Theory (TD-DFT) calculations and B3LYP method which is the hybrid functional Becke, three-parameter, Lee-Yang-Parr [44,45] with an effective core potential basis set LANL2DZ [69–72] of the calculated UV–visible absorption, was in agreement with the experimental results. It is worth noting that previous studies were demonstrated the capability of chosen method and basis set to predict the electronic properties of metallic complexes quite reasonably [73–76]. For example, the calculated absorption spectrum of the complex ZnL1 (Fig. 15) showed in the ultraviolet domain two bands due to the intra-ligand transitions π → π*. Another band located at 400 nm corresponded to the metal–ligand charge transfer.

The ligand coordination sites that were involved in bonding with the metal ions have been determined by careful comparison of the infrared absorption spectra of the complexes with that of the parent ligand. The vibrational assignments were carried out with support DFT calculations using the Minnesota M06 global hybrid meta-GGA functional [77] with LANL2DZ basis set [78,79]. The experimental and theoretical FT-IR spectra of CuL1 were given in Fig. 16 (see supplementary information). The IR spectra indicate that the ligand was coordinated through the O (of –OH) and N (of –NH) atoms of L1 and the N-atoms from the

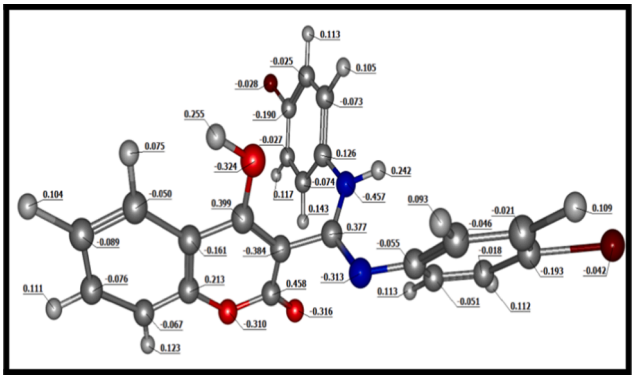

Fig. 14. Optimized Geometry, the Mulliken atomic charges distribution and calculated thermodynamics parameters: Enthalpy = $-3968.99.10^3$ Kcal/mol of the ligand L1.

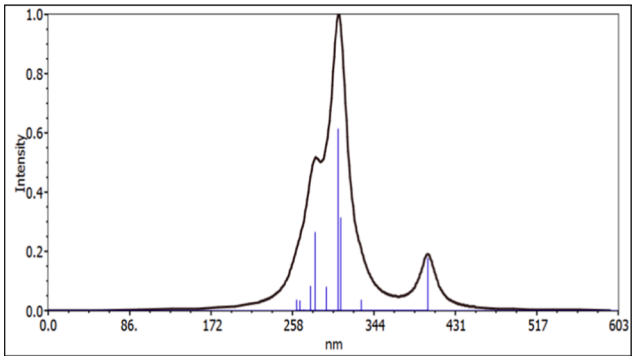

Fig. 15. Theoretical absorption spectra of ZnL1.

ammoniac moiety, resulting in neutral species.

On basis of the elemental analysis, NMR, electronic spectra and theoretical studies, the complexes were formulated as $[ML_1(NH_3)_2Cl_2]H_2O$ (Fig. 17).

In order to study the stability of the synthesized complexes, their binding energy have been calculated (Table 5). The lowest value of the binding energy corresponded to the most stable complex. Analysis of these results shows that the CoL1 complex had the highest binding energy value, which indicated that this complex was the least stable. On the other hand, CuL1 and ZnL1 complexes have the lowest binding energies indicating that these complexes were the most stable.

3.6. Conductivity

The conductimetric measurements of the complexes were performed in DMSO at a concentration of 1×10^{-3} M. The results showed that the complexes are non-electrolytes. The analytical data and physical properties of the complexes were summarized in Table 6.

3.7. Electrochemical: Cyclic voltammetry study

The electrochemical properties of free ligand **L_1** and its complexes of copper, zinc and cobalt were investigated. The redox potentials, ΔEp (difference between the anodic peak potential and the cathodic peak potential) and the Ipa/Ipc ratios (Ipa = anodic peak current, Ipc = peak current cathode) obtained are classified in Table 7.

The voltammogram of the free ligand L1 (Fig. 18) was registered on a tension field going of −2000 and +1500 mV/SCE at a scanning rate v = 100 mV/s. The ligand L_1 present one peak of reduction at −551 mV/SCE and tow oxidation peaks at −495 mV/SCE and 93 mV/SCE. The cathodic peak corresponds to the reduction of imine group and the low peaks anodic were attributed to the oxidation of the imine and phenolic groups.

The voltammogram obtained for the CuL1 complex (Fig. 19), in the anodic direction, displayed three oxidation peaks p_a (I), (p_a (II) and p_a (III) corresponding to the potential values Ep_a equal to −449 mV/SCE, −1479 mV/SCE and 167 mV/SCE respectively. In the cathodic direction, it showed tow peaks of reduction p_c (I) and p_c (II) corresponding to the potential values Epc equal to −559 mV/SCE and −1289 mV/SCE. The anodic process corresponding to peak p_a (I) and peak p_a (III) can only be the result of a redox process of ligand L1. The other peak (peak 2) observed in Fig. 19 was supposed to be the result of an oxidation and reduction occurring at the level of the Cu (II) ion [80]. In the negative potential range and on the cathode scan, the peak attributed to the metal shown by the cyclic voltammogram of the complex was intense. However, when scanning in the opposite direction, the anode peak related to the cathode wave was not intense. This indicated that during cathodic reduction, the electrode process was complicated by a chemical reaction.

During a scan ranging from + 1500 mV to −2000 mV, the Co (II) complex has two shallow cathodic responses in the form of a shoulder at about −585 mV and −1408 mV and three localized anodic peaks at −351 mV, −1501 mV and 210 mV. On the cathodic scan, the reduction peak located at −1408 mV and the oxidation peak displayed at −1501 mV were attributed to the redox pair Co (II)/Co (I) [81]. The rest of the peaks correspond to oxidation and reduction at the ligand center (see Fig. 20, supplementary information).

The electrochemical response of the Zn (II) complex shown on the cyclic voltammogram (Fig. 21, see supplementary information) showed on the cathodic scan two oxidation–reduction processes and on the anodic scan an oxidation peak without a cathodic response. A reduction wave was observed within the range of the studied potential attributed to the reduction of the Zn (II) metal ion to Zn (I). The Ipa/Ipc ratio of 0.46 far from unity indicated irreversible behavior.

Table 5
Calculated binding energies of synthesized metallic complexes at the DFT level of theory.

	CoL1	CuL1	ZnL1
|EB| (eV)	11,70	10,34	11,16

Table 6
Analytical and physical data of the investigated compounds.

Comp.	Yield	Color and aspect	Pf (°C)	$\Lambda\ \Omega^{-1}.cm^2.mol^{-1}$ In DMSO
$[Cu(L1)(NH_3)_2Cl_2]H_2O$	61	Green powder	˃260	10.51
$[Co(L1)(NH_3)_2Cl_2]H_2O$	58	Dark red powder	˃260	5.43
$[Zn(L1)(NH_3)_2Cl_2]H_2O$	67	White yellowish powder	˃260	9.32

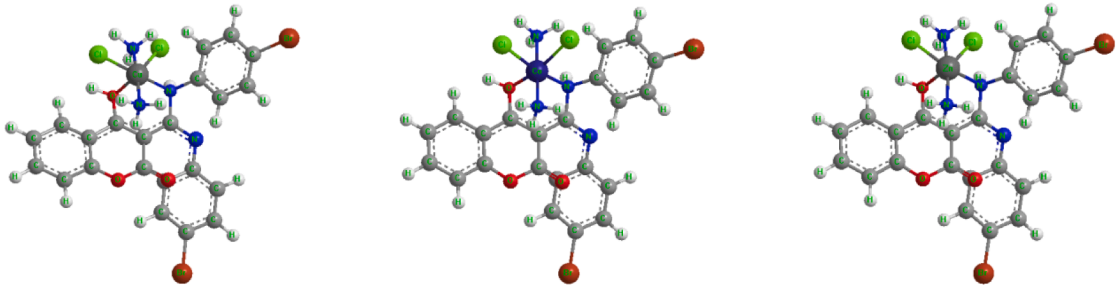

$[Cu(L1)(NH_3)_2Cl_2]H_2O$ $[Co(L1)(NH_3)_2Cl_2]H_2O$ $[Zn(L1)(NH_3)_2Cl_2]H_2O$

Fig. 17. Proposed structures for L1 complexes.

Table 7
Cyclic voltametry data for Ligand L1 complexes.

Compound	Epc [V]	Ipc (mA)	Epa [V]	Ipa (mA)	ΔEP [V]	$E_{1/2}$(V)	ipa/ipc
L1	−0.551	−0.044	−0.495	0.059	0.056	−0.523	1.34
			0.093	0.037			
CuL1			0.167	0.041			
	−0.559	−0.024	−0.449	0.032	0.110	−0.504	1.33
	−1.289	−0.175	−1.479	0.012	−0.190	−1.384	0.07
CoL1			0.210	0.060			
	−0.585	−0.025	−0.376	0.039	0.209	−0.480	1.56
	−1.408	−0.086	−1.501	0.025	−0.093	−1.454	0.29
ZnL1			0.604	0.092			
	−0.640	−0.033	−0.430	0.053	0.210	−0.535	1.60
	−1.169	−0.145	−1.057	0.066	0.112	−1.113	0.46

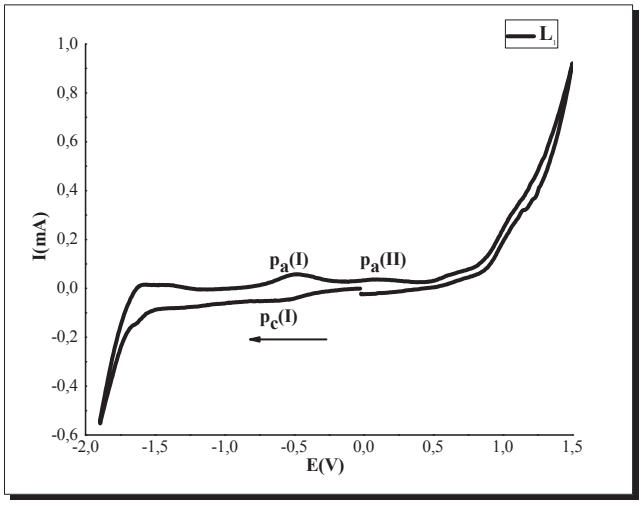

Fig. 18. Cyclic voltamogramm of L1 (10^{-3} M) in DMSO (100 mV s^{-1} scan rate). The arrows show the peak positions.

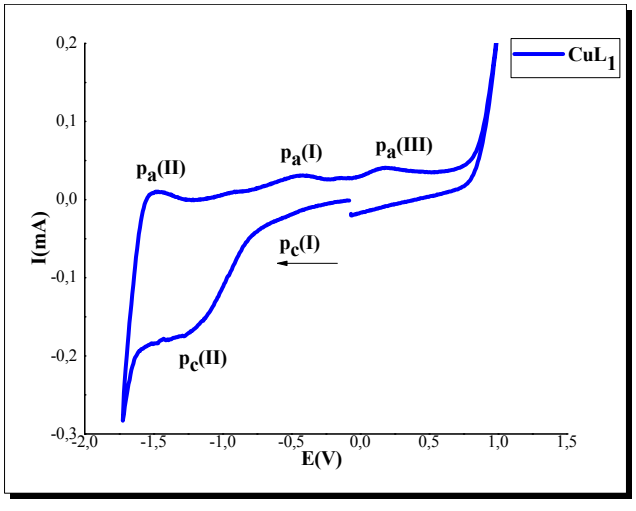

Fig. 19. Cyclic voltamogramm of CuL1 (10^{-3} M) in DMSO (100 mV s^{-1} scan rate). The arrows show the peak positions.

3.8. Antimicrobial activity

A comparative evaluation of the antimicrobial activity of L1 and the synthesized complexes was carried out against one Gram-positive (*S. Aureus*) bacteria and two Gram-negative bacteria (*E. Coli* and *P. Aeruginosa*). The results obtained were presented in Table 8 and illustrated in Fig. 22 (see supplementary information). The result

Table 8
Range of diameters inhibition zones (mm) for the ligand L1, the complexes and the reference antibiotic (Gentamicin 10 μg).

Bacterial	Diameters of inhibition zones (in mm)				
	L1	CuL1	CoL1	ZnL1	ATB
S. Aureus	**13**	**6**	17	**17**	**20**
	++	-		++	++
E. Coli	**11**	**6**	**6**	**11**	**22**
	+	-	+	+	+++
P. Aeruginosa	**10**	**10**	**9**	**9**	**18**
	+	+	-	+	++

The sensitivity of microorganisms, toward tested compounds, was identified in the following manner: no activity ($- \leq 8$ mm), slightly active ($8 < + < 16$ mm), moderately active ($16 \leq ++ \leq 20$ mm) and highly active ($+++ > 20$ mm). ATB: antibiotic

indicated a moderate activity of L1 with respect to the three bacteria. This activity varied in the case of complexes according to the nature of the metal. All the complexes except that of copper showed good activities against the *S. Aureus* and those of cobalt and zinc had very interesting diameters of inhibition. Copper and cobalt complexes were inactive against *E.Coli*, but in the case of zinc, the activity was the same as the ligand L1. The activity of the copper, cobalt and zinc complexes against *P. Aerugenosa* remains the same as that of the ligand L1. The results also showed that the complexes had an enhanced activity compared to the ligand itself. This is especially shown against *S.Aureus*. Finally the metal activity decreases in the order Zn > Co > Cu.

3.9. Antioxidant activity

The antioxidant activity of the ligand L1 and its complexes was measured in terms of their hydrogen donating or radical scavenging ability by UV–visible spectrophotometer using the stable 2,2-diphenyl-1-picrylhydrazyl radical ($DPPH^{\cdot}$). Fig. 23 shows the variation of absorbance versus concentration of the ligand L1 and the different complexes (Fig. 23a, see supplementary information) and of the standard ascorbic acid (Fig. 23b, see supplementary information). The lower the absorbance of the reaction mixture indicates the higher free radical scavenging activity (RSA). The capability to scavenge the DPPH (as % of inhibition) was calculated using Eq. (1).

The ligand L1 exhibited higher scavenging activity than its corresponding complexes. It is very interesting to note that RSA of the synthesized compound L1 is greater than the one of ascorbic acid (standard). This high activity was probably due to the presence of the OH group. The decrease of the antioxidant activity of the complexes is due to the low oxidation potential of the metal ions, which can easily release an electron to participate in the reduction of DPPH. Minimum inhibitory concentrations IC50 of the tested compounds are illustrated in Fig. 24.

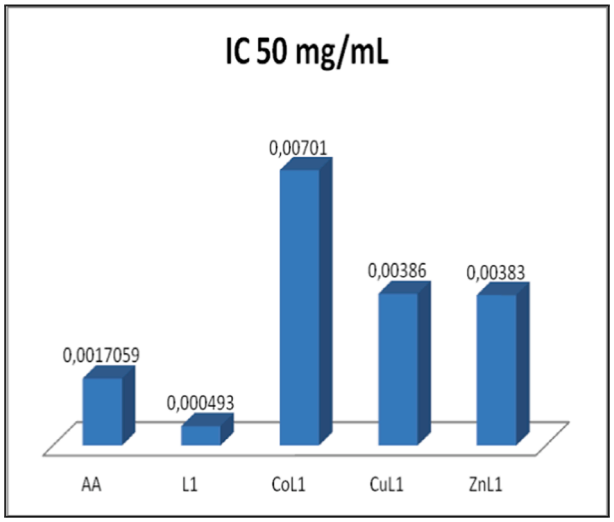

Fig. 24. IC50 (mg/mL) values of the antioxidant compounds tested.

4. ADMET and drug-likeness analysis

In silico ADMET analysis was performed to verify if the synthesized complexes and ligands present any toxicity through the human body. Table 9 reports predicted pharmacological and ADMET properties of synthesized ligands and metallic complexes. Analysis of results showed that studied compounds were predicted as non-AMES-toxic (AMEST), and non-carcinogenic. It is worth noting that's AMES toxicity represents an excellent measure of bacterial mutagenicity. In addition, all complexes were predicted as weak Human Ether-a-go-go-Related Gene (hERG) blockers. It is important to remember that hERG potassium channel plays a central role in regulating cardiac excitability and maintenance of normal cardiac rhythm. Thus, hERG channel blockade can cause cardiac arrythmia. Additionally, most synthesized compounds are a non-Permeability-glycoprotein (PG) and non-Cytochrome P450 inhibitors for most isoforms such as CYP2C19, CYP2D6, CYP3A4 and CYP2C9. The cytochrome P450 proteins play a vital role in metabolism and an inhibition of its isoforms would lead to drug interactions, accumulation and toxicity [82]. Interestingly, most of the synthesized compounds showed positive values of Blood-brain barrier penetration (BBB) [83].

Additionally, all compounds demonstrated good pharmacokinetic profile in human intestinal absorption (HIA), which could allow them to reach the site of action. All synthesized compounds showed poor penetration to colorectal carcinoma permeability (**Caco-2)**. The octanol–water partition coefficient (Log p = -0,4 – 5,6), which usually quantified molecular lipophilicity, and Total Polar Surface Area (TPSA ≤ 160), a good indicator of the bioavailability of the drug molecule, were in the acceptable ranges. Therefore, all synthesized compounds pass the verber rule defined as TPSA and number of rotatable bond less than 140 Å and 10, respectively [84].

5. Conclusion

In this work, N,N'-di(4-bromophenyl)-4-hydroxycoumarin-3-carboximidamide L1 and N-(4-Bromophenyl)-4-hydroxycoumarin-3-carbothioamide L2 were synthesized and structurally characterized by FT-IR, mass spectrometry, elemental analyses and NMR spectroscopy. It was shown that the probes N, N'-di(4-bromophenyl)-4-hydroxycoumarin-3-carboximidamide L1 and N-(4-Bromophenyl)-4-hydroxycoumarin-3-carbothioamide L2 are sensitive to the presence of metal cations. The pectroscopic properties of these dyes allowed us to show that strong interactions take place between L1 (and L2) and d-metal cations in DMSO solutions, at very low concentrations of product and salts. This result was established using complementary techniques: absorption and emission spectrophotometry, as well as semi-empirical calculations.

In view of the high affinity of the ligand for d-metal cations, this work could lead to the design of new photoactive sensors potentially useful for chemical or biomedical analysis.

We have prepared a series of three metal complexes of *N,N'*-di(4-bromophenyl)-4-hydroxycoumarin-3-carboximidamide L1. These complexes were characterized using instrumental techniques and confirmed the complexation and the presence of metals. Furthermore, they were evaluated as antioxidant and antimicrobial agents showing, for the complexes, a reduced antioxidant power and an improved antimicrobial activity compared to L1. It worth of note that among of the three complexes, those with cobalt and zinc showed the best antimicrobial activity.

These results were supported by theoretical studies. ADMET and drug likeness analyses showed that most compounds have satisfactory pharmacokinetics and drug like parameters values.

Table 9
ADMET properties of synthesized ligands (L1a, L1b, L2) and metallic complexes (CuL1, CoL1 and ZnL1) predicted by admetSAR and SwissADME web servers.

Property	L1a	L1b	L2	CuL1	CoL1	ZnL1
AMEST	Non	Non	Non	Non	Non	Non
Carcinogenic	Non	Non	Non	Non	Non	Non
hERG	Weak	Weak	Weak	Weak	Weak	Weak
PG Inhibitor	Non	Yes	Non	Non	Non	Non
CYP2C19	Non	Yes	Non	Non	Non	Non
CYP2D6	Yes	Non	Non	Non	Non	Non
CYP3A4	Non	Non	Yes	Non	Non	Non
CYP2C9	Non	Yes	Yes	Non	Non	Non
BBB	+	–	–	+	+	+
HIA	+	+	+	+	+	+
Caco-2	poor	poor	poor	poor	poor	poor
Log P	5.19	4.76	3.55	3.83	3.52	3.52
TPSA (Å^2)	78.83	67.43	94.56	81.31	81.31	81.31
Verber rule	Yes	Yes	Yes	Yes	Yes	Yes

Author agreement

All authors have seen the final version of the manuscript and approved the same before submission.

Declaration of Competing Interest

The authors declare that they have no known competing financial interests or personal relationships that could have appeared to influence the work reported in this paper.

Acknowledgments

Thanks are due to University of Aveiro and FCT/MEC for the financial support of the QOPNA research unit (FCTUID/QUI/00062/2013) through national founds and, where applicable, co-financed by the FEDER, within the PT2020 Partnership Agreement, and to the Portuguese NMR Network. We would like to thank the Ministry of Higher Education and Scientific Research of Algeria for awarding an exchange scholarship.

Appendix A. Supplementary material

Supplementary data to this article can be found online at https://doi.org/10.1016/j.inoche.2021.108509.

References

[1] Z.Y. Pan, Dr. C. P. Tan, L.S. Rao, H. Zhang, Y. Zheng, L. Hao, Prof. Liang-Nian Ji, Prof. Zong-Wan Mao, Recoding the Cancer Epigenome by Intervening in Metabolism and Iron Homeostasis with Mitochondria-Targeted Rhenium(I)

Complexes, Angew. Chem. Int. Edit. 59 (42) (2020) 18556-18562. https://doi.org/10.1002/anie.202005362.
[2] Dr. Q. Cao, D.J. Zhou, Z.Y. Pan, Dr. G.G. Yang, H. Zhang, Prof. Liang-Nian Ji, Prof. Zong-Wan Mao, Recoding the Cancer Epigenome by Intervening in Metabolism and Iron Homeostasis with Mitochondria-Targeted Rhenium(I) Complexes, Angew. Chem. Int. Edit. 59 (42) (2020) 18755-18762. https://doi.org/10.1002/anie.202008624.
[3] Shao-Mei Zhang, Hai-Yang Zhang, Qi-Pin Qin, Jia-Wei Fei, Shu-Hua Zhang, Syntheses, crystal structures and biological evaluation of two new Cu(II) and Co(II) complexes based on (*E*)-2-(((4H–1,2,4-triazol-4-yl)imino)methyl)-6-methoxyphenol, J. Inorgan Biochem. 193 (2019) 52–59, https://doi.org/10.1016/j.jinorgbio.2019.01.009.
[4] Z. Guo, J. Jin, Z. Xiao, N. Chen, X. Jiang, X. Liu, L. Wu, Y. He, S. Zhang, Four iron (II) carbonyl complexes containing both pyridyl and halide ligands: Their synthesis, characterization, stability, and anticancer activity, Appl. Organometal Chem. 35 (1) (2021), e6045, https://doi.org/10.1002/aoc.6045.
[5] C. Xing, Y. Fang, L. Jiang, Y. Zhang, M. Li, Diorganotin(IV) complexes derived from *N*-terminal methylation of Triapine: synthesis, characterization and antibacterial activity evaluation, J. Organomet. Chem. 911 (2020), 121153, https://doi.org/10.1016/j.jorganchem.2020.121153.
[6] Y.T. Wang, Y. Fang, M. Zhao, M.X. Li, Y.M. Ji, Q.X. Han, Cu(II), Ga(III) and In(III) complexes of 2-acetylpyridine *N*(4)-phenylthiosemicarbazone: synthesis, spectral characterization and biological activities, Med. Chem. Commun. 8 (2017) 2125–2132, https://doi.org/10.1039/C7MD00415J.
[7] A.C. Stein, S. Alvarez, C. Avancini, S. Zacchino, G. Von Poser, J. Ethnopharm. 107 (2006) 95–98.
[8] M. Kawase, N. Motohasi, H. Sagakami, T. Kanamoto, H. Nakashima, L. Fereczy, K. Walfard, C. Miskolci, J. Molnar, Int. J. Antimicrob. Agents. 18 (2001) 161–165.
[9] F. Borges, F. Roleira, M. Milhazes, L. Santana, E. Uriate, Curr. Med. Chem. 12 (2005) 887–916.
[10] H. Sheibani, M.R. Islami, H. Khabazzadeh, K. Saidi, Tetrahedron 60 (2004) 5931–5934.
[11] S. Ma, S. Yu, S. Yin, J. Org. Chem. 68 (2003) 8996–9002.
[12] T. Yao, R.C. Larock, J. Org. Chem. 68 (2003) 5936–5942.
[13] M. Biagetti, F. Bellina, A. Carpita, R. Rossi, Tetrahedron Lett. 44 (2003) 607–610.
[14] S. Rousset, M. Abarbri, J. Thibonnet, J.-L. Parrain, A. Duchêne, Tetrahedron Lett. 44 (2003) 7633–7636.
[15] J. Louie, J.E. Gibby, M.V. Farnworth, T.N. Tekavec, J. Am. Chem. Soc. 124 (2002) 15188–15189.
[16] J. Thibonnet, M. Abarbri, J.L. Parrain, A. Duchêne, J. Org. Chem. 67 (2002) 3941–3944.
[17] R. Rossi, F. Bellina, M. Biagetti, A. Catanese, L. Mannina, Tetrahedron Lett. 41 (2000) 5281–5286.
[18] X.-F. Zhu, A.P. Schaffner, R.C. Li, O. Kwon, Org. Lett. 7 (2005) 2977–2980.
[19] W.R. Huck, T. Mallat, A. Baiker, New J. Chem. 26 (2002) 6–8.
[20] M.J. Fehr, G. Consiglio, M. Scalone, R. Schmid, J. *Org. Chem.* 64 (1999) 5768–5776.
[21] N. Halland, T. Velgaard, K.A. Jorgensen, J. Org. Chem. 68 (2003) 5067–5074.
[22] A.D. Kulkarni, G.B. Bagihalli, S.A. Patil, P.S. Badami, Synthesis, characterization, electrochemical and *in vitro* antimicrobial studies of Co(II), Ni(II) and Cu(II) complexes with Schiff bases of formyl coumarin derivatives, J. Coord. Chem. 62 (2009) 3060–3072.
[23] (a) J. Patel, H. Dholariya, K. Patel, J. Bhatt, K. Patel. Cu(II) and Ni(II) complexes of coumarin derivatives with fourth generation flouroquinolone: synthesis, characterization, microbicidal and antioxidant assay. Med. Chem. Res. 23 (8) (2014) 3714–3724. DOI 10.1007/s00044-014-0943-y. (b) S. Radha, K. K. Mothilal, A. Thamaraichelvan and R. Shanmugam. Synthesis, Characterization, Antimicrobial and Density Functional Theory Studies of Metal Complexes of 3-Benzoyl-7-methoxy Coumarin, Ind. J. Pharm. Sci. 80 (4) (2018) 619-627. DOI: 10.4172/pharmaceutical-sciences.1000401.
[24] R.D. Thornes, L. Daly, G. Lynch, B. Breslin, H. Browne, H.Y. Browne, T. Corrigan, P. Daly, G. Edwards, E. Gaffney, J. Henley, T. Healy, F. Keane, F. Lennon, N. McMurray, S. O'Loughlin, M. Shine, A. Tanner, Treatment with coumarin to prevent or delay recurrence of malignant melanoma, J. Cancer. Res. Clin. Oncol. 120 (1994) 32–34, https://doi.org/10.1007/BF01377122.
[25] M.E. Marshall, J.L. Mohler, K. Edmonds, B. Williams, K. Butler, M. Ryles, L. Weiss, D. Urban, A. Bueschen, M. Markiewicz, G. Cloud, An updated review of the clinical development of coumarin (1,2-benzopyrone) and 7-hydroxycoumarin, J. Cancer Res. Clin. Oncol. 120 (1994) 39–42, https://doi.org/10.1007/BF01377124.
[26] J.L. Mohler, B.T. Williams, I.M. Thompson, M.E. Marshall, Coumarin (1,2-benzopyrone) for the treatment of prostatic carcinoma, J. Cancer Res. Clin. Oncol. 120 (1994) 35–38.
[27] O. Dömötör, T. Tuccinardi, D. Karcz, M. Walsh, B.S. Creaven, E.A. Enyedy, Interaction of anticancer reduced Schiff base coumarin derivatives with human serum albumin investigated by fluorescence quenching and molecular modelling, Bioorg. Chem. 52 (2014) 16–23.
[28] B.G. Lake, Coumarin metabolism, toxicity and carcinogenicity: Relevance for human risk assessment, Food. Chem. Toxicol. 37 (4) (1999) 423–453.
[29] M.E. Marshall, K. Butler, A. Fried, Phase I evaluation of coumarin (1,2-benzopyrone) and cimetidine in patients with advanced malignancies, Mol. Biother. 3 (3) (1991) 170–178.
[30] M.E. Marshall, K. Kervin, C. Benefield, A. Umerani, S. Albainy-Jenei, Q. Zhao, et al., Growth-inhibitory effects of coumarin (1,2-benzopyrone) and 7-hydroxycoumarin on human malignant cell lines *in vitro*, J. Cancer Res. Clin. Oncol. 120 (1994) 3–10.
[31] R.B. Myers, M. Parker, W.E. Grizzle, The effects of coumarin and suramin on the growth of malignant renal and prostatic cell line, J. Cancer Res. Clin. Oncol. 120 (1994) 11–13.
[32] S. Kawaii, Y. Tomono, K. Ogawa, M. Sugiura, M. Yano, Y. Yoshizawa, The antiproliferative effect of coumarins on several cancer cell lines, Anticancer Res. 21 (2001) 917–923.
[33] G. Gasser, Metal complexes and medicine: A successful combination, Chimia 69 (7) (2015) 442–446.
[34] M.P. Sathisha, U.N. Shetty, V.K. Revankar, K.S.R. Pai, Synthesis and antitumor studies on novel Co(II), Ni(II) and Cu(II) metal complexes of bis(3-acetylcoumarin) thiocarbohydrazone, Eur. J. Med. Chem. 43 (11) (2008) 2338–2346.
[35] D. Belkhir-Talbi, M. Makhloufi-Chebli, S. Terrachet-Bouaziz, D. Hikem-Oukacha, N. Ghemmit, L. Ismaili, A.M.S. Silva, M. Hamdi, Synthesis, characterization, theoretical studies, ADMET and drug-likeness analysis: Electrochemical and biological activities of metal complexes of 3-(2-hydroxybenzoyl)-2*H*-chromen-2-one, J. of Molec. Struc. 1179 (2019) 495–505.
[36] M. Makhloufi-Chebli, M. Hamdi, A.M.S. Silva, O. Duval, J.J. Helesbeux, 2*H*-pyran-2-one-3-carbothioamide derivatives: synthesis and reaction with hydrazine hydrate, J. Het. Chem. 46 (2009) 18–22.
[37] Vogel's Fifth Edition, practical organic chemistry, P.P 967.
[38] G.G.F. Nascimento, J. Locatelli, P.C. Freitas, G.L. Silva, Braz. J. Microbiol. 31 (2000) 247–256.
[39] J.S. Lee, H.J. Kim, H. Park, Y.S. Lee, J. Nat. Prod. 65 (2002) 1367–1370.
[40] L.L. Mensor, F.S. Menezes, G.G. Leitão, et al., Phytother Res. 15 (2001) 127–130.
[41] Marvin Sketch (version 18.28.0), calculation module developed by Chem Axon, http://www.chemaxon.com/products/marvin/marvinsketch/, 2014.
[42] F. Neese, The ORCA program system" Wiley interdisciplinary Reviews - Computational Molecular Science, 2 (2012) 73-78.
[43] F. Neese, Calculation of the zero-field splitting tensor on the basis of hybrid density functional and Hartree-Fock theory, J. Chem. Phys. 127 (16) (2007) 164112–164119.
[44] A.D. Becke, Density-functional exchange-energy approximation with correct asymptotic behavior, Phys. Rev. A Gen. Phys. 38 (1988) 3098–3100, https://doi.org/10.1103/physreva.38.3098.
[45] C. Lee, W. Yang, R.G. Parr, Development of the Colle-Salvetti correlation-energy formula into a functional of the electron density, Phys. Rev. B 37 (1988) 785–789, https://doi.org/10.1103/physrevb.37.785.
[46] S. Grimme, J. Antony, S. Ehrlich, H. Krieg, J. Chem. Phys. 132 (15) (2010), 154104, https://doi.org/10.1063/1.3382344.
[47] A.R. Allouche, Gabedit-A graphical user interface for computational chemistry softwares, J. Comput. Chem. 32 (1) (2011) 174–182, https://doi.org/10.1002/jcc.21600.
[48] T. Lu, F. Chen, J. Comp. Chem. 33 (5) (2012) 580–592, https://doi.org/10.1002/jcc.22885.
[49] H. Van de Waterbeemd, E. Gifford, ADMET *in silico* modelling: towards prediction paradise, Nat. Rev. Drug Discov. 2 (3) (2003) 192–204.
[50] C.H. Andrade, D.C. Silva, R.C. Braga, *In silico* prediction of drug metabolism by P450, Curr. Drug Metab. 15 (2014) 514–525.
[51] F. Cheng, W. Li, Y. Zhou, J. Shen, Z. Wu, G. Liu, P.W. Lee, Y. Tang, J. Chem. Inf. Model. 52 (11) (2012) 3099–3105.
[52] N. Bruce, Ames Science, 249 (4976) (1990) p.1487; DOI: 10.1126/science.249.4976.1487-a.
[53] A. Lagunin, D. Filimonov, A. Zakharov, W. Xie, Y. Huang, F. Zhu, T. Shen, J. Yao, V. Poroikov, QSAR Comb. Sci. 28 (2009) 773–928, https://doi.org/10.1002/qsar.200860192.
[54] F. Broccatelli, E. Carosati, A. Neri, M. Frosini, L. Goracci, T.I. Oprea, G. Cruciani, J. Med. Chem. 54 (2011) 1740–1751.
[55] R.G. Susnow, S.L. Dixon, J. Chem. Inf. Comput. Sci. 43 (4) (2003) 1308–1315, https://doi.org/10.1021/ci030283p.
[56] R. Liu, H. Sun, S.S. So, J. Chem. Inf. Comp. Sci. 41 (2001) 1623–1632.
[57] G. Klopman, L.R. Stefan, R.D. Saiakhov, Eur. J. Pharm. Sci 17 (2002) 253–263.
[58] J.A. Castillo-Garit, Y. Marrero-Ponce, F. Torrens, R. Garcia-Domenech, J. Pharm. Sci. 97 (2008) 1946–1976.
[59] R.A.W. Johnstone, B.J. Millard, F.M. Dean, A.W. Hill, J. Chem. Soc. (C) (1966) 1712–1717.
[60] R.N. Porter, J. Baldas, Mass Spectrometry of heterocyclic Compounds, Wiley-Interscience, New York, 1985, p. 214.
[61] S. Koç, D.A. Köse, E. Avici, Eur. Chem. Bull 5 (4) (2016) 132–137.
[62] N. Tidjani-Rahmouni, N. Bensiradj, S. Djebbar, O. Benali-Baitich, J. Mol. Struct. 1075 (2014) 254–263.
[63] S. Alghool, J. Coord. Chem. 63 (2010) 3322–3333.
[64] R. Fazlur, Complex Metals 1 (2014) 88–95.
[65] S. Rehman, Z. Chohan, F. Gulnaz, C. Supuran, J. Enzyme Inhib. Med. Chem. 20 (4) (2005) 333–340.
[66] R.I.H. AL-Bayati, F.R. Mahdi, A.A.H. Al-Amiery, Br. J. Pharmacol. Toxicol., 2(1) (2011) 5-11.
[67] T. Aiyelabola, E. Akinkunmi, E. Obuotor, I. Olawuni, D. Isabirye, J. Jordaan, Bioinorg. Chem. Appl. 2017 (2017) 1–9.
[68] W. Szcze, P. Panik, P. Mlynarz, M.K. Stefanowicz, N.D. Kalminska, A.O. Amelis, A. Mjkut, M. Ratajska Staszewska, M.G. Bojczuk, Structural studies of Cu(II) binding to the novel peptide derivative of quinoxaline glycine, Polyhedron 30 (1) (2011) 9–15.
[69] Modern Theoretical Chemistry vol. 3 (1976) 1.
[70] P.J. Hay, W.R. Wadt, J. Chem. Phys. 82 (1985) 270–283.
[71] P.J. Hay, W.R. Wadt, J. Chem. Phys. 82 (1985) 284–298.
[72] P.J. Hay, W.R. Wadt, J. Chem. Phys. 82 (1985) 299–310.

[73] S.I. Gorelsky, A.B.P. Lever, J. of Organomet. Chem. 635 (2001) 187–196.
[74] D. Polyansky, D. Cabelli, J.T. Muckerman, E. Fujita, T.A. Koizumi, T. Fukushima, T. Wada, K. Tanaka, Angew *Chem. Int. Ed. Engl.* 46 (2007) 4169–4172.
[75] C.E. Check, T.O. Faust, J.M. Bailey, B.J. Wright, T.M. Gilbert, L.S. Sunderlin, J. Phys. Chem. A 105 (2001) 8111–8116.
[76] E.W.S. Caetano, U.L. Fulco, E.L. Albuquerque, A.H. de Lima Costa, S.N. Costa, A. M. Silva, F.A.M. Sales, V.N. Freire, J. Phys. Chem. Sol. 121 (2018) 36–48.
[77] Y. Zhao, D.G. Truhlar, The M06 suite of density functionals for main group thermochemistry, thermochemical kinetics, noncovalent interactions, excited states, and transition elements: Two new functionals and systematic testing of four M06-class functionals and 12 other functionals, Theor. Chem. Acc. 120 (1–3) (2006) 215–241, https://doi.org/10.1007/s00214-007-0310-x.
[78] W.J. Hehre, R.F. Stewart, J.A. Pople, Self-consistent molecular orbital methods. 1. Use of Gaussian expansions of slater-type atomic orbitals, J. Chem. Phys. 51 (1969) 2657–2664, https://doi.org/10.1063/1.1672392.
[79] J.B. Collins, P.R. Schleyer, J.S. Binkley, J.A. Pople, Self-consistent molecular orbital methods, 17. Geometries and binding energies of second-row molecules. A comparison of three basis sets, J. Chem. Phys. 64 (1976) 5142–5151, https://doi.org/10.1063/1.432189.
[80] S. Tabti, M. Benmahmoud, A. Djedouani, L. Semmar, A. Hamimid, Synthesis, characterization and electrochemical behavior of new transition metal complexes derivatives of 4-hydroxy-6-methyl-3-[(2E)-3-(4(dimethylamino) phenyl) prop-2-enoyl]-2*H*-pyran-2-one, J. Mater. Environ. Sci. 9 (9) (2018) 2624–2630.
[81] A.D. Kulkarni, S.A. Patil, P.S. Badami, Electrochemical properties of some transition metal complexes: synthesis, characterization and in-vitro antimicrobial studies of Co(II), Ni(II), Cu(II), Mn(II) and Fe(III) complexes, Int. J. Electrochem. Sci. 4 (2009) 717–729.
[82] T. Lynch, D. Pharm, A. Price, The effect of cytochrome P450 metabolism on drug response, interactions, and adverse effects, Am. Fam. Physician. 76 (2007) 391–396.
[83] A. Iraji, O. Firuzi, M. Khoshneviszadeh, H. Nadri, N. Edraki, R. Miri, Synthesis and structure-activity relationship study of multi-target triazine derivatives as innovative candidates for treatment of Alzheimer's disease, Bioorg. Chem. 77 (2018) 223–235, https://doi.org/10.1016/j.bioorg.2018.01.017.
[84] D.F. Verber, S.R. Johnson, H.Y. Cheng, B.R. Smith, K.W. Ward, K.D. Kopple, J. Med. Chem. 45 (12) (2002) 2615–2623.